JGR Oceans

RESEARCH ARTICLE
10.1029/2024JC022245

Effect of Climate Change-Induced Tropical Cyclone Track Shift on Sedimentology in the East China Coastal Ocean

Chaoran Xu[1,2], Yang Yang[3], Mingxiao Xie[1], Jeremy D. Bricker[4,5], Fan Zhang[2], Ya Ping Wang[2], Xiaoliang Xia[6], and Jianjun Jia[2]

[1]National Engineering Research Center of Port Hydraulic Construction Technology, Tianjin Research Institute for Water Transport Engineering, Tianjin, China, [2]State Key Laboratory of Estuarine and Coastal Research, School of Marine Sciences, East China Normal University, Shanghai, China, [3]School of Marine Science and Engineering, Nanjing Normal University, Nanjing, China, [4]Department of Civil and Environmental Engineering, University of Michigan, Ann Arbor, MI, USA, [5]Faculty of Civil Engineering & Geosciences, Delft University of Technology, Delft, The Netherlands, [6]Ningbo Hangzhou Bay Bridge Development Co., Ltd., Ningbo, China

Abstract Tropical cyclones (TCs) significantly influence coastal sedimentation, geomorphologic features, and morphodynamic processes through strong winds, heavy rains, and storm surges. These effects are particularly pronounced in the east China coastal ocean. However, the impacts of poleward and landward shifts in TC tracks on sedimentology, specifically sediment transport and erosion-deposition processes, remain insufficiently understood. This study utilizes the Delft3D-FM numerical model integrated with TC best track data and field measurements to investigate sediment transport patterns under historical TC tracks and to quantify erosion responses to poleward and landward track shifts. From the historical sediment transport pattern derived from the typical historical TC track, results reveal that sediment in waters shallower than 30 m is highly sensitive to TC activity, with four distinct zones where net sediment transport is sensitive to the change of typical historical TC tracks. Coastal erosion depth changes due to poleward and landward shifts of typical TC tracks during the peak TC intensity period are quantified as 0.24–1.63 cm°N^{-1} and 0.05–1.06 cm°E^{-1}, respectively. Under global warming scenarios, these values are projected to increase by 2.45%–8.00% and 4.71%–13.33%, respectively. Identifying the coastal areas more susceptible to TC-induced sediment transport and quantitatively assessing the effects of poleward and landward track shifts are important for understanding local TC variability and supporting research on sedimentology during TCs and the future protection of coastal areas.

Plain Language Summary Tropical cyclones (TCs) greatly affect coastal areas through strong winds, heavy rains, and storm surges. These impacts are especially noticeable along the east China coastal ocean. However, the effect of changes in TC tracks, such as moving northward or inward, on sediment transport and erosion is not fully understood. This study uses a numerical model along with TC data and field measurements to explore sediment transport under historical TC tracks and measure erosion from changes in TC tracks. The results show that sediment in waters less than 30 m deep is very responsive to TC activity, with four main zones of active sediment transport. Coastal erosion varies with TC track shifts, ranging from 0.24 to 1.63 cm per degree northward shift and 0.05–1.06 cm per degree eastward shift. Under climate change, these values could increase by 2.45%–8.00% and 4.71%–13.33%. Identifying areas most vulnerable to TC-induced changes helps in understanding TC impacts and improving coastal protection strategies.

Key Points:

- Four areas in the east China coastal ocean are sensitive to changes in sediment transport caused by TCs
- The sensitivity of erosion to latitudinal and longitudinal changes along the east China coastal ocean ranged from 0.24–1.63 cm°N^{-1} to 0.05–1.06 cm°E^{-1}, respectively
- Under global warming, these latitudinal and longitudinal changes will be enhanced by 2.45%–8.00% and 4.71%–13.33%, respectively

Supporting Information:

Supporting Information may be found in the online version of this article.

Correspondence to:

M. Xie and J. Jia,
crabsaver@163.com;
jjjia@sklec.ecnu.edu.cn

Citation:

Xu, C., Yang, Y., Xie, M., Bricker, J. D., Zhang, F., Wang, Y. P., et al. (2025). Effect of climate change-induced tropical cyclone track shift on sedimentology in the east China coastal ocean. *Journal of Geophysical Research: Oceans*, *130*, e2024JC022245. https://doi.org/10.1029/2024JC022245

Received 10 DEC 2024
Accepted 29 MAY 2025

Author Contributions:

Conceptualization: Mingxiao Xie, Jianjun Jia
Data curation: Chaoran Xu, Mingxiao Xie, Jianjun Jia
Methodology: Chaoran Xu, Yang Yang, Mingxiao Xie, Jeremy D. Bricker
Project administration: Mingxiao Xie, Jianjun Jia
Software: Chaoran Xu
Writing – original draft: Chaoran Xu
Writing – review & editing: Yang Yang, Mingxiao Xie, Jeremy D. Bricker, Fan Zhang, Ya Ping Wang, Xiaoliang Xia, Jianjun Jia

1. Introduction

Tropical cyclones (TCs) are one of the most destructive extreme weather events, causing significant social and economic impacts on coastal cities (Helderop & Grubesic, 2019; Li & Chakraborty, 2020; Muis et al., 2016; Wang et al., 2021). The direct economic losses caused by TC-induced storm surges in the east China coastal ocean (ECCO) are the highest and most volatile in this region (Xu, Yang, et al., 2022). Therefore, understanding the effects of TC variation, especially on a regional scale in the ECCO, is an important topic. Anthropogenic global warming has caused temperatures more than 1°C warmer than before industrialization, and this warming trend will continue to increase in the future (Calvin et al., 2023; IPCC, 2022). Global warming is also changing the state of TC generation and development (Emanuel, 1986, 2003), resulting in earlier generation and development of intense TCs (Shan et al., 2023), and increased duration over land, allowing for increased TC impacts on land (Knutson et al., 2019). Additionally, the lifetime maximum intensity (LMI) of TCs is undergoing a poleward

(Kossin et al., 2014, 2016; Studholme et al., 2022) and landward shift (Wang & Toumi, 2021). Although the frequency of global TCs is decreasing (Zhao et al., 2024), an increasing number of TCs affecting the South China Sea are migrating northeastward, increasing the number of TCs affecting the ECCO, with a clear trend of poleward and landward shift in this region (Xu et al., 2024; Zhao et al., 2014). As a result, the ECCO is exposed to increased disaster risk from the effects of TCs. Strong winds during TCs, as well as waves, can cause significant increases in current velocities and seabed shear stresses, leading to sediment resuspension, increases in suspended sediment concentration (SSC) (Hawkes & Horton, 2012), and changes in seabed sediment transport patterns (Schuerch et al., 2014). This can cause substantial impacts on deltaic erosion and sediment redistribution on the coast (Liu et al., 2023; Lu et al., 2018). Due to the fine grain size of seabed sediments, the hydrodynamic forces caused by TCs in nearshore waters of the ECCO (with water depths of less than 40 m) can cause severe erosion or accretion in the short term (Dai, Liu, Wei, & Chen, 2014; Du et al., 2019), which is of great importance to the sediment dynamics of the shallow waters of the continental shelf (Zhu et al., 2020).

Storm surges caused by TCs can lead to marine hazards such as coastal erosion and harbor siltation in this region. Currently, there are many studies on the hydrodynamic aspects of extreme water levels and inundation risks caused by TCs (Guo et al., 2023; Mo et al., 2024; Wang et al., 2021), but the analysis of sediment transport patterns and erosion-deposition trends caused by TCs is mostly focused only on certain economically developed coastal areas, or the analysis of disaster recurrence after a TC (Ren et al., 2021; Yin et al., 2019). Currently, the impacts of poleward and landward shifts of TCs on sedimentology in the ECCO area, particularly concerning net sediment transport patterns caused by typical historical TCs and erosion-deposition processes, remain poorly understood. There is a notable lack of studies quantitatively assessing sedimentology resulting from the spatial and temporal changes of TCs. Hypothetical storm tracks representing typical historical TCs can be used to determine typical sediment transport patterns during different historical periods, in a way that conserves computational resources. Identifying which coastal areas are more susceptible to TCs and quantitatively analyzing such effects are urgent challenges. Understanding this variable response is important for the future protection of coastal areas. However, field sampling and observation during TCs require a lot of material and financial resources, and observation is difficult. Therefore, integrating numerical simulations with analyses of measured data offers an effective approach to studying the spatial and temporal characteristics of TCs and their sedimentology effects in the ECCO, while ensuring accuracy.

This study focuses on the effects of TC changes on sediment transport and erosion-deposition processes in sedimentology. In this study, the Delft3D-FM model is used to simulate the variability in sediment transport and erosion-deposition processes during different TCs in the ECCO over a long period by combining the spatial and temporal data of historical TC meteorology with sediment data. From the historical sediment transport patterns caused by typical TCs, we determine which coastal areas are more susceptible to TCs and analyze the quantitative relationship between changes in TC characteristics and changes in erosion and deposition patterns. It is of great theoretical significance and engineering application value to understand the impacts of spatial and temporal variations of localized TCs and to improve the disaster prevention and mitigation capability of response-sensitive coastal areas in response to TCs.

2. Materials and Methods

2.1. Study Area

The study area ranges from 25.5°N–32.0°N to 119.5°E–124.0°E (Figure 1), which contains the Yangtze River Estuary, Hangzhou Bay, and the Zhejiang-Fujian coast. This area is severely affected by TCs. This region, with its dense population and rapidly growing economy, is highly vulnerable to natural disasters, leading to significant annual losses due to tropical cyclones (Wang & Song, 2011; Xu & Huang, 2011). For example, Typhoon Winnie caused 186 deaths and over 22.9 billion yuan in damage in the Jiangsu, Shanghai, and Zhejiang provinces in 1997 (SOA, 1997). Meanwhile, the shelf in this region is one of the most extensive in the world and has a fine-grain-dominated sedimentary system (Gao & Collins, 2014). This area is an ideal region for conducting storm deposition research (Gao et al., 2019). Analyzing the spatiotemporal variation of TCs and the response of sediments provides a reference for storm deposition studies in this region.

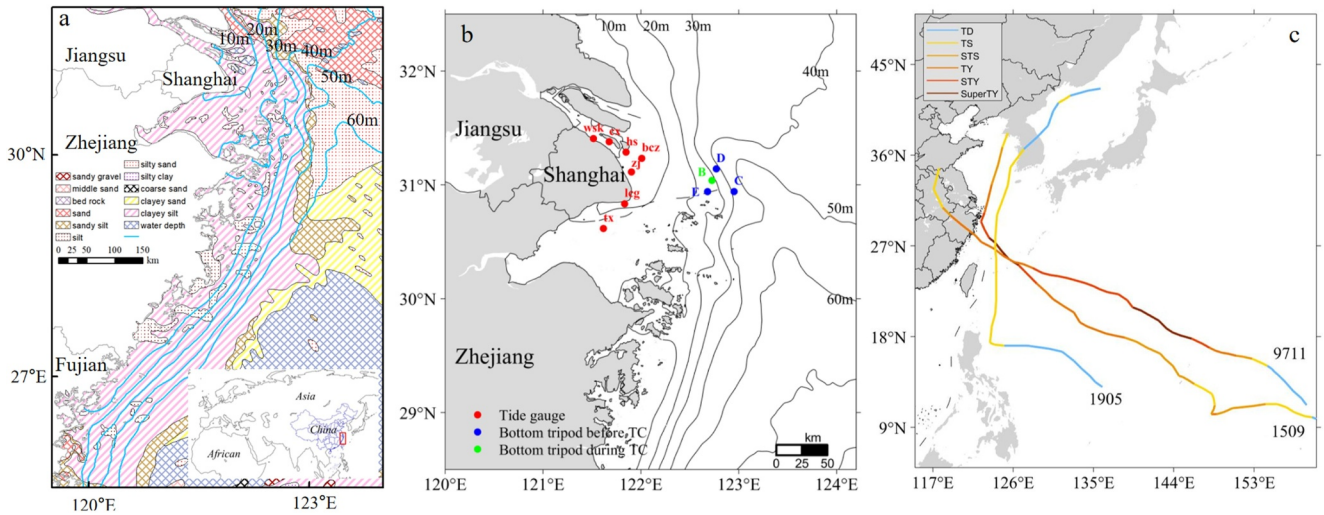

Figure 1. Study area (a) shows the surface sediment type in the ECCO (adapted from Shi, 2012). (b) Indicates the locations of hydrodynamic observation sites. The observed data at site B were collected during Typhoon 1905 (Danas-2019), while data at sites C, D, and E were obtained before Typhoon 1905. Data at sites wsk, cx, hs, bcj, zj, lcg, and tx were recorded during Typhoon 9711 (Winnie-1997). (c) Illustrates the tracks of Typhoon 9711, Typhoon 1509 (Chan-hom-2015), and Typhoon 1905. Abbreviations are as follows: wsk, Wusongkou; cx, Changxing; hs, Hengsha; bcj, Beicaozhong; zj, Zhongjun; lcg, Luchaogang; tx, Tanxu; TD, tropical depression; TS, tropical storm; STS, severe tropical storm; TY, typhoon; STY, severe typhoon; and SuperTY, supertyphoon.

2.2. Data Sources

The TC track data used in this study is from the Shanghai Typhoon Institute of the China Meteorological Administration (CMA) (Lu et al., 2021; Ying et al., 2014). It contains each TC center's longitude, latitude, time, maximum wind speed, and minimum pressure at 6-hr intervals.

The observed data during Typhoon 1905 (Danas-2019) at four sites (Figures 1b and 1c) are from Tang et al. (2023). It contains the water level, SSC, bottom elevation, waves, and velocity data. The observed data during Typhoon 9711 (Winnie-1997) at seven sites are from Ren et al. (2021) and Xu, Tian, et al. (2022). It contains the storm tide and wind speed data.

Two topography data sets were used to build the model: the General Bathymetric Chart of the Oceans (GEBCO, 15 arc s) for the deep sea and high-resolution bathymetry from nautical chart digitization near the coast (mean sea level datum). Astronomical tides (K1, O1, Q1, P1, M2, S2, N2, and K2 on the open boundaries are applied as harmonics from the OTIS regional and global tidal models (Egbert & Erofeeva, 2002). Because the downstream reach of the Yangtze River is included in the model, river discharge data as well as the river's SSC were obtained from the China River Sediment Bulletin. The critical shear stress data used in the sediment module were determined from two data sets (see Section 2.3.2): measured data from sediment samples using a cohesive strength meter (CSM) and calculated based on sediment grain size using an existing empirical formula (Guo, 2020; Xu, Wei, et al., 2022).

2.3. Numerical Model Setup

2.3.1. Tropical Cyclone Model

Reanalysis data sets are too coarse to resolve TC maximum winds, and so underestimate the wind and pressure during TCs while also showing bias for the location of the TC centers (Schenkel & Hart, 2012). Parametric TC models calculate more accurate wind and pressure fields near the TC eyewall and are more suitable for the storm surge simulation. The Delft3D WES (Wind Enhance Scheme) is an integrated module within the Delft3D dashboard software. It utilizes TC best track data and applies the Holland formula (Holland, 1980, 2008) to generate wind and pressure fields in the Spiderweb format (Deltares, 2022a). Delft3D WES considers asymmetry by taking into account the translational speed of the TC center displacement due to the steering flow, as well as rotation of the wind velocity due to friction (Takagi & Wu, 2016). Wind and pressure fields generated by Delft3D WES are widely used as input to Delft3D-FM models (Ke et al., 2021; Xu et al., 2022, 2023).

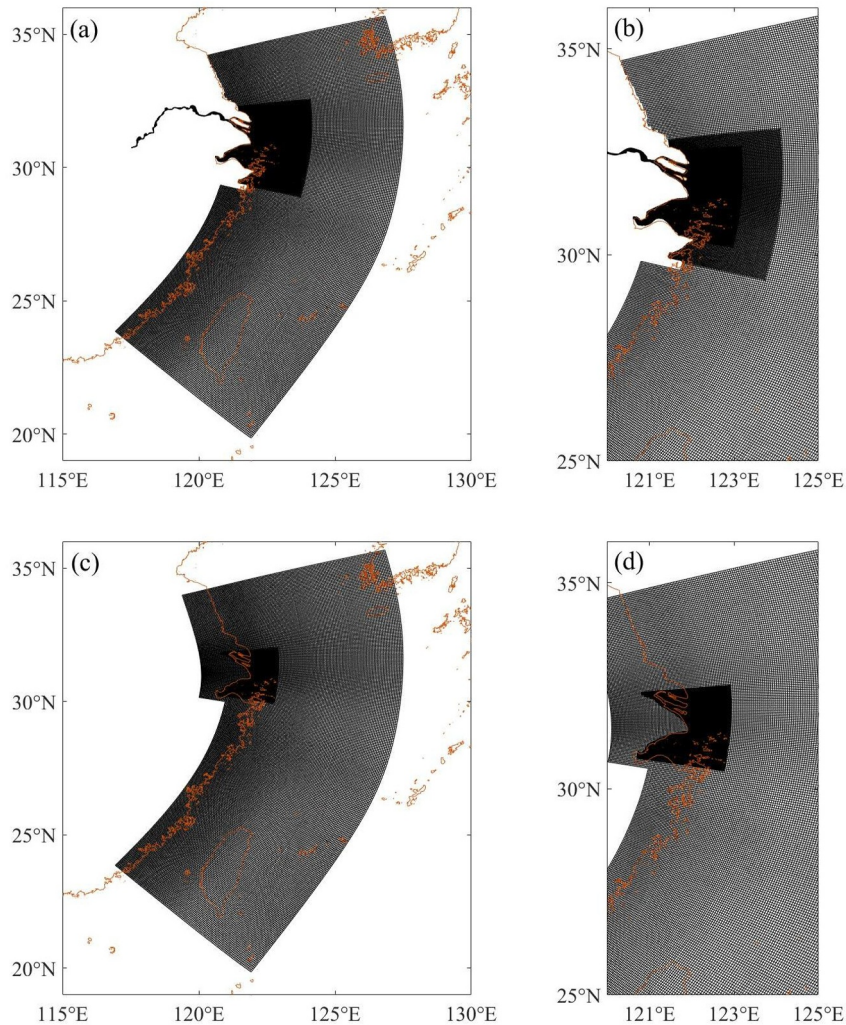

Figure 2. The simulation regions and grids for the flow and wave models. (a) Is the flow module grid, (b) is the locally enlarged flow model region, (c) is the wave module grid, and (d) is the locally enlarged wave model region.

2.3.2. Delft3D-FM Flow-Wave Coupling Model Setup

The Delft3D-FM model suite used in this study is a two-dimensional model. It applied in depth-averaged mode and solves the nonlinear shallow water equations for unsteady flow, which are derived from the Navier-Stokes equations for incompressible free surface flow (Deltares, 2022a). A dynamic time-stepping approach is employed, where the model determines the time step for each computational iteration to maintain stability based on the Courant number criterion. Additionally, it integrates the third-generation wave model, Simulating Waves Nearshore (SWAN), a spectral wave model designed to solve the wave action balance equation (Deltares, 2022b). Delft3D-FM is capable of simulating tidal circulation and the propagation of storm surges in complex coastal environments, and it is widely used in modeling flow and waves during TCs (Al-Attabi et al., 2023; Diaz Loaiza et al., 2022; Ke et al., 2021; Veeramony et al., 2017; Xu et al., 2022, 2023; Zou et al., 2020).

The computational domain of the model extends from 20.0°N–35.5°N to 116.5°E–127.5°E (Figure 2). The flow module uses an unstructured grid that gradually increases in cell size from about 400 m in the estuary to about 10,000 m at the open boundary, totaling 110,435 elements (Figures 2a and 2b). The wave module adopts a structured grid with higher resolution in the estuarine area using nested grids, with the number of large cells being 280 × 171 at a resolution of 5,000–10,000 m, and the number of small cells being 353 × 293 at a resolution of 500 m (Figures 2c and 2d).

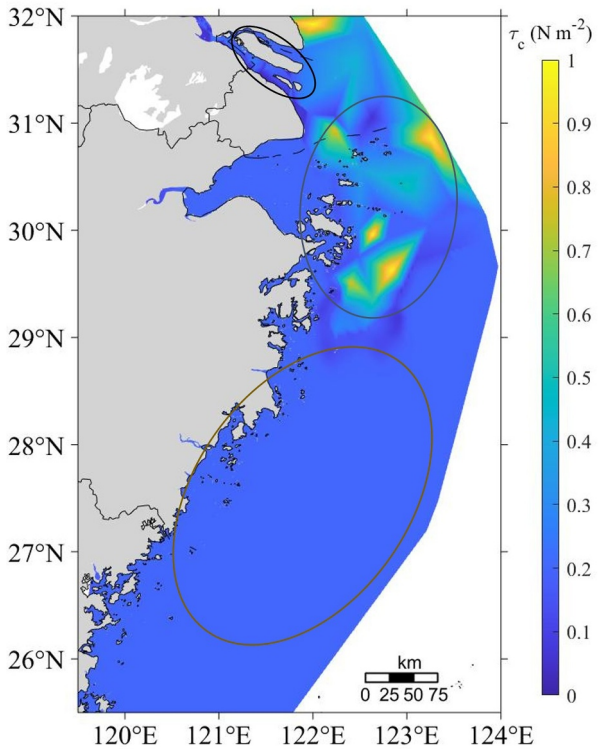

Figure 3. Spatial distribution of critical shear stress in model. The three ellipses from north to south indicate critical shear stresses calculated by the empirical formula near the Yangtze estuary, the CSM-measured result in the subaqueous delta, and the constant value of critical shear stress off the Zhejiang and Fujian coasts, respectively.

The simulation time is based on the duration of the TC in the region of interest. A constant Manning's n of 0.02 m s$^{-1/3}$ was used for the bottom roughness after model validation. This is a typical value used for the seabed. The air-sea drag coefficient was modeled using a trilinear relation: 0.0012 (0–28 m/s), 0.003 (28–60 m/s), and 0.0015 (>60 m/s) (Makin, 2005; Xu, Xing, et al., 2023). The discharge boundary and initial SSC of the Yangtze River mouth adopts a multiyear average runoff and sediment load of 30,000 m^3 s^{-1} and 0.11 kg m^{-3} at Datong Station (30.11°N, 117.13°E), respectively. The rest of the parameter settings use default values (Deltares, 2022a). The wave module is evaluated in nonstationary mode, and the other parameters use default values (Deltares, 2022b). The flow and wave modules are coupled online at 60-min intervals.

Sediments in coastal sea areas, such as shallow shelves, tidal flats, coastal wetlands, and lagoons, are susceptible to TCs. Therefore, it is important to accurately characterize the nearshore sediment properties in the model. A series of previous studies have proven that the sediments in the specified study area are dominated by cohesive sediments; hence, the sediment fractions in the numerical model are set as a single cohesive type. The most important parameter is the critical shear stress for sediment erosion. The critical shear stress of the coarser grain sediments at the mouth of the Yangtze River (Chen et al., 2021) was calculated using an empirical formula based on the median grain size of the sediments (Guo, 2020). The sediments in the Yangtze River subaqueous delta and its neighboring seas are dominated by fine-grained cohesive sediments, such as silt and clay, for which the critical shear stress is difficult to accurately express by empirical formulas, so values from CSM measurements are used (Xu, Wei, et al., 2022). And the critical shear stress for deposition and erosion are the same. The southern part of the study area is a muddy area along the coast of Zhejiang and Fujian, where the sediment grain size is fine and uniformly distributed (Shi, 2012), so the critical shear stress in this area was set to 0.2 N m^{-2} based on CSM measurements (Figure 3). The dry bed density was set to 1,600 kg m^{-3} based on measured data and model calibration (Xue et al., 2020). The erosion rate was set to 2×10^{-5} kg m^{-2} s^{-1} after model calibration. A simple flocculation model was used in this study to determine sediment settling velocity, where fine-grained, cohesive sediment undergoes flocculation and settles at a rate that is directly related to water salinity. Flocculation occurs when the salinity exceeds 8 psu (Hu et al., 2009) and the maximum settling velocity is set to 1 mm s^{-1}.

2.3.3. Model Validation

In this study, we conducted a comprehensive validation of several key parameters during two distinct typhoon events. For Typhoon 9711, we validated the water level and wind speed. During Typhoon 1905, we measured multiple parameters at station B (Figure 1b), including significant wave height, wave period, wave-current combined shear stress, SSC, current speed and direction, and bed elevation changes. Additionally, we analyzed bed elevation changes at stations C, D, and E before Typhoon 1905.

The model's accuracy was quantitatively assessed using two statistical metrics: root mean square error (RMSE, Equation 1) and the skill number (Equation 2). The skill number, ranging from 0 to 1, provides a robust measure of model performance. Following the classification established by Willmott (1981), model performance was categorized as follows: optimal (1), excellent (0.65–1), good (0.5–0.65), average (0.2–0.5), and poor (<0.2). This systematic evaluation framework ensures a rigorous assessment of model reliability and shows the validated results by the Taylor diagram (Figure 4); please refer to the supporting information for detailed validation (Table S1 and Figures S1–S5 in Supporting Information S1).

$$\mathrm{RMSE} = \sqrt{\frac{\sum_{i=1}^{n}(M_i - S_i)^2}{n}} \quad (1)$$

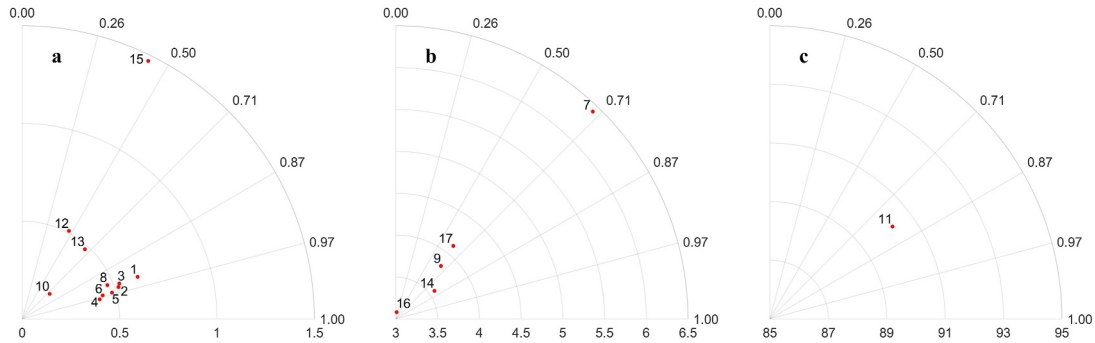

Figure 4. The validated result on the Taylor diagram. The *x*-axis is root mean square error, and the circular axis is the skill number; the station number 1–17 can be found in Table S1 in Supporting Information S1. (a) Is the validation of storm tide, significant wave height, velocity speed, bed shear stress, and SSC; (b) is the validation of peak wave period and bed elevation change; and (c) is velocity direction.

$$\text{skill} = 1 - \frac{\sum_{i=1}^{n} |M_i - S_i|^2}{\sum_{i=1}^{n} \left(|M_i - \overline{S}| + |S_i - \overline{S}| \right)^2} \tag{2}$$

where, M and S represent the modeled and observed values, respectively, $\overline{S}$ is the average of the observed values, and n is the number of observed values.

The modeled values are in high agreement with the observed values, indicating the model results are reliable (Figure 4). Although the bed elevation change data at station B were partly missing during Typhoon 1905, the overall trend is similar and of the same magnitude. Analysis of nonstorm bed elevation changes at stations C, D, and E shows that while the skill number is poor at C and D, the model captures the observed trend. The fluctuations at C and D likely stem from a stable seabed with a surface layer of highly erodible mud. In contrast, station E exhibits strong agreement between modeled and observed trends, reflecting more stable bed behavior. The simulation of sediment transport processes is more challenging than hydrodynamic processes and sensitive to the choice of parameterization scheme. The validation results demonstrate that the model is effective and suitable for simulating and analyzing erosion-deposition patterns.

2.4. Tropical Cyclone Scenarios Construction

2.4.1. Construction of TCs With Different Typical Tracks

Combining the TC wind field distribution and the M-K trend test method, TCs affecting the ECCO between 1949 and 2022 are divided into three historical periods (Xu, Yang, et al., 2022). Then, combining the methods of mass moment, mean cluster, and track interpolation for each TC eye, the TCs in each period are divided into three main types of characteristic tracks, namely a northwest track (I), a northwest-northeast turning track (II), and a northwest-northeast turning offshore track (III) (Xu et al., 2024). Therefore, the TC tracks affecting this region can be generalized to 9 typical tracks (Figure 5). Differences in conditions such as TC track, intensity, and duration over the past 70 years can have a significant impact on sediment transport patterns. Because only the latitude, longitude, and wind speed of the TC center are available in the classification of TC tracks, the 9 typical tracks do not include time and pressure information (Xu et al., 2024). Therefore, to simulate the sediment transport process caused by the 9 typical tracks, it is necessary to artificially assign the full information of the TC centers. The 9 typical TCs were assigned the full information based on validated Typhoon 9711 intensities to become 9 complete hypothetically constructed TCs. Then, 9 hypothetically constructed TCs (the black tracks in Figure 5) are simulated using Delft3D-FM to analyze the overall sediment transport patterns from the TC impacts during each of the historical periods, and to determine the areas in the ECCO that are sensitive to the response of TC-induced sediment transport processes.

2.4.2. Construction of TCs With Different Longitude and Latitude Based on Typical TC

Globally, TC tracks are undergoing poleward and landward migration (Kossin et al., 2014; Shan et al., 2023; Wang & Toumi, 2021). TCs affecting the ECCO have shifted poleward by 1.26° in latitude and landward by 0.66°

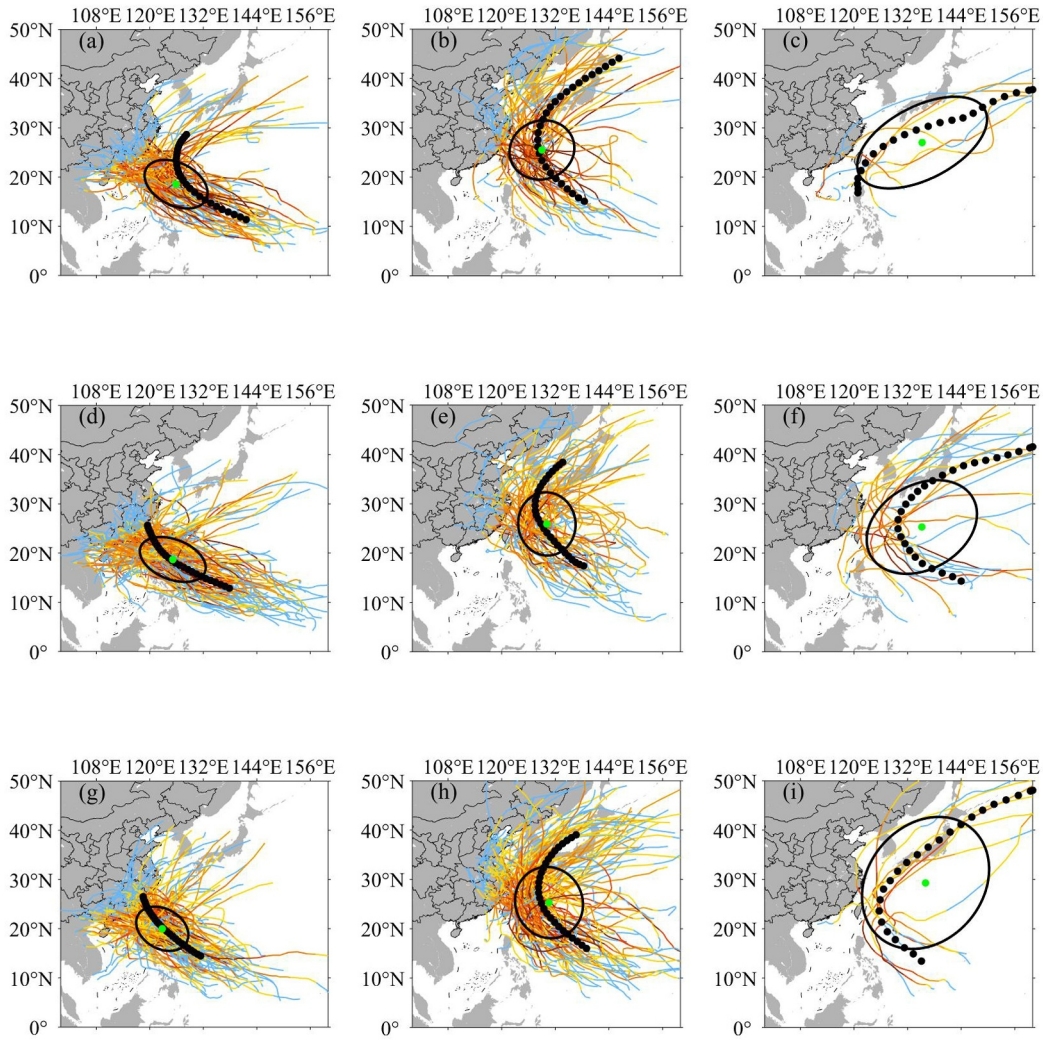

Figure 5. Typical TC track for each TC cluster during three historical periods (Xu et al. (2024)). (a–c) Are type I, II, and III tracks in 1949–1967, (d–f) are type I, II, and III tracks in 1968~1993, and g–i are type I, II, and III tracks in 1994–2022. The green dots are mean centroid locations, the black circles are mean-variance ellipses, the black dots are typical TC tracks, and the colored lines in panels (a–i) are individual TC tracks.

in longitude (Xu et al., 2024) throughout the historical record. This trend of poleward and landward shift will increase the TC disaster risk for the ECCO in the future. It is important to construct different scenarios of latitudinal and longitudinal variations of TC tracks to quantitatively understand the sedimentology induced by changes in TC tracks.

The two most significant tracks affecting the ECCO are hypothetical track I and track II. It can be seen from their locations that the development of typical TC track I displays a landward migration (longitudinal change) with time, showing a continuous progression toward the shore. Therefore, the impact of latitudinal changes under this typical track I will be more prominent, and are suitable for analyzing latitudinal migration. The development of typical TC track II displays a poleward migration (latitudinal change), showing a continuous progression toward the north. Therefore, the impact of longitudinal changes under this typical track II will be more prominent and suitable for analyzing longitudinal migration. Typhoon 9711 which belongs to track I had a very serious impact on the ECCO; Typhoon 1509 which belongs to track II caused 7.99×10^6 m^3 of sudden siltation in the deepwater channel at the mouth of the Yangtze River (Jia et al., 2017) (Figure 1c). Therefore, 10 experimental scenarios were designed based on the degree of latitudinal and longitudinal shift of historical TCs, latitudinal migration adjusted to 1°, and longitudinal migration adjusted to 0.7° based on Xu et al. (2024) (Table 1, Figure 6):

Table 1
Scenarios Based on Typhoon 9711 and Typhoon 1509 With Changes in Latitude and Longitude

Typhoon	Changes in latitude and longitude (°)	Scenario name
Typhoon 9711 latitude change setup	+0	A1
	+1	A2
	+2	A3
	+3	A4
	+4	A5
Typhoon 1509 longitude change setup	+0	B1
	+0.7	B2
	+1.4	B3
	+2.1	B4
	+2.8	B5

1. Numerical simulations to investigate the effect of northward shift of latitude based on the track of Typhoon 9711, changing the latitude of the center of Typhoon 9711 in steps of 1°, obtaining 5 scenarios.
2. Numerical simulations to investigate the effect of the westward shift of longitude based on the track of Typhoon 1509, changing the longitude of the center of Typhoon 1509 in steps of 0.7°, obtaining 5 scenarios.

2.4.3. Construction of TCs Under Global Warming

The Intergovernmental Panel on Climate Change (IPCC) AR6 has estimated that the global warming caused by human activities is irreversible (Calvin et al., 2023). With a global temperature increase of 2°C, the maximum wind speeds of TCs increase by about 5% (Knutson et al., 2020). There is a proportional relationship between TC center pressure deficit and wind speed (Atkinson & Holliday, 1977) (Equation 3)

$$V_m = \mathrm{a}(1015 - P_0)^{\mathrm{b}} \tag{3}$$

where V_m (m s^{-1}) is the maximum wind speed near the TC eyewall, P_0 (hPa) is the TC center's pressure, and a and b are the fitting coefficients.

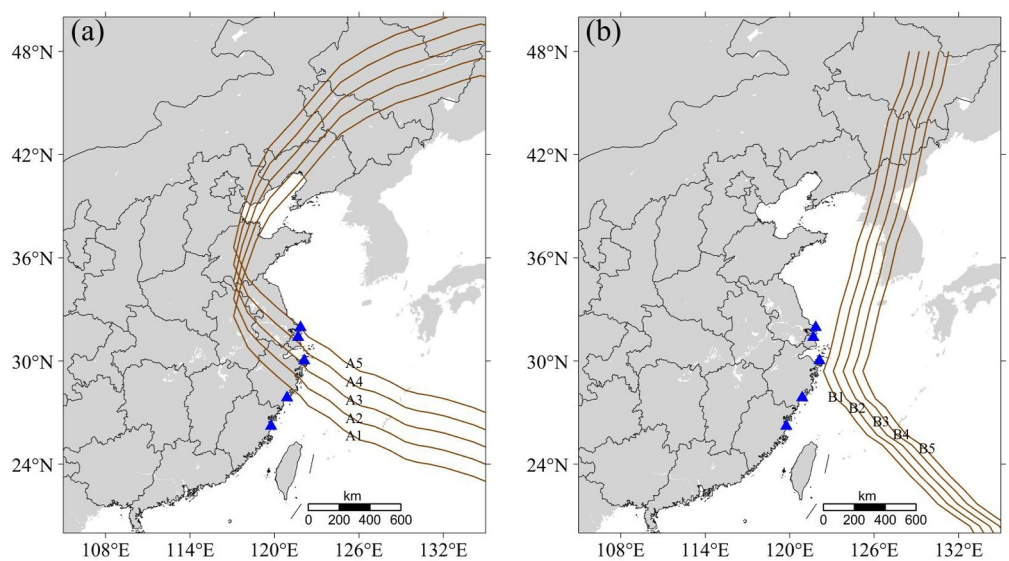

Figure 6. Spatial distribution of TC track scenarios. (a) Is the track of Typhoon 9711 for the latitudinal change scenarios and (b) is the track of Typhoon 1509 for the longitudinal change scenarios. The blue triangles from north to south are the five coastal observation points of Qidong, Hengsha, Zhoushan, Wenzhou, and Fuzhou, respectively.

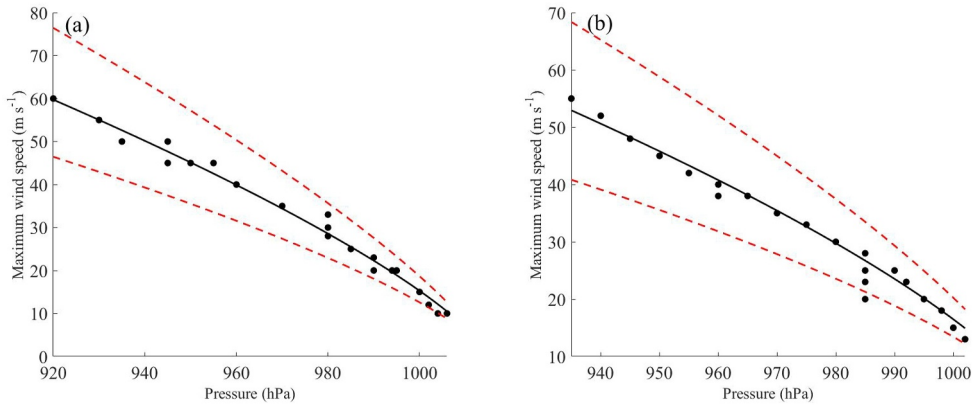

Figure 7. The relationships between maximum wind speed and pressure for Typhoon 9711 and Typhoon 1509. (a) Is the wind-pressure relationship for Typhoon 9711, and (b) is the wind-pressure relationship for Typhoon 1509; the black solid line is the fitted trend, and the red dashed lines are the 95% confidence intervals.

Thus, global warming will lead to an increase in the intensity of TCs. Global warming will also incur a rise in global sea level, which will rise by up to 1.1 m by the year 2100 under a high carbon dioxide emission scenario (RCP8.5), with an increase in temperature of about 4°C (Calvin et al., 2023; IPCC, 2022). Therefore, varying the TC intensity and water depth is an effective way to analyze the different impacts caused by TCs under global warming (Guo et al., 2023).

Based on the above studies, we assume that a warming of 4°C will increase the maximum wind speed in the 10 scenarios in Section 2.4.2 by 10%. We then use Equation 3 to calculate the wind-pressure relationships for Typhoon 9711 and Typhoon 1509 (Figure 7), and then calculate the increase in TC center pressure deficit based on the increase in wind speed. The initial water depth in the model is increased by 1.1 m (Calvin et al., 2023; IPCC, 2022) to account for the effect of sea level rise, and a total of 10 new scenarios under global warming conditions are obtained.

3. Results

3.1. Net Sediment Transport Pattern Under Typical Historical TCs

Net sediment transport reflects the sediment balance of a region and is mainly controlled by tidal currents and strongly influenced by local topography and extreme events (Xing et al., 2024; Xu, Xing, et al., 2023). To eliminate the effect of periodic tides, a low-pass filtering method (the cutoff frequency is 34 hr in this study) was used to process the flow to obtain the residual current (Thompson, 1983; Walters & Heston, 1982). Flux decomposition theory (Dyer, 1997) is then used to derive the net sediment transport (Xing et al., 2024; Xu, Xing, et al., 2023). This section employs a controlled variable approach to analyze the response of net sediment transport in the ECCO to changes in the typical TC tracks from different historical periods while keeping other inputs of the model the same. The aim is to identify which regions exhibit significant sensitivity to these typical TC track variations, thereby demonstrating the potential impact of future trends in TC activity on specific areas and then focusing on monitoring tropical cyclone activity in these identified regions. The distribution of net sediment transport flux caused by three typical TCs during the three periods is shown in Figures 8–10. The magnitude of net sediment transport flux caused each TC of the same track type is similar, while the magnitude caused by TCs with different track types varies.

From the net sediment transport pattern in each historical period, we find that there are four areas where the net sediment transport is sensitive to TC type (Figures 8–10, the brown dashed areas from left to right). First, the shallow area of the Yangtze River Delta with water depth of 20 m or less, and especially the area with a water depth of 10 m or less in the southern branch of the Yangtze River Estuary, has the most active sediment transport, and the direction of net sediment transport is mainly to the northeast along the estuary. The net sediment flux in Hangzhou Bay is weaker. The sediment transport activity in the area shallower than 10 m at the head of Hangzhou Bay is the most active area in the bay, and the net sediment transport direction is along the bay. Sediment transport is also active in the area with a water depth of 20–30 m to the east of the Zhoushan Islands. Along the Ningbo-

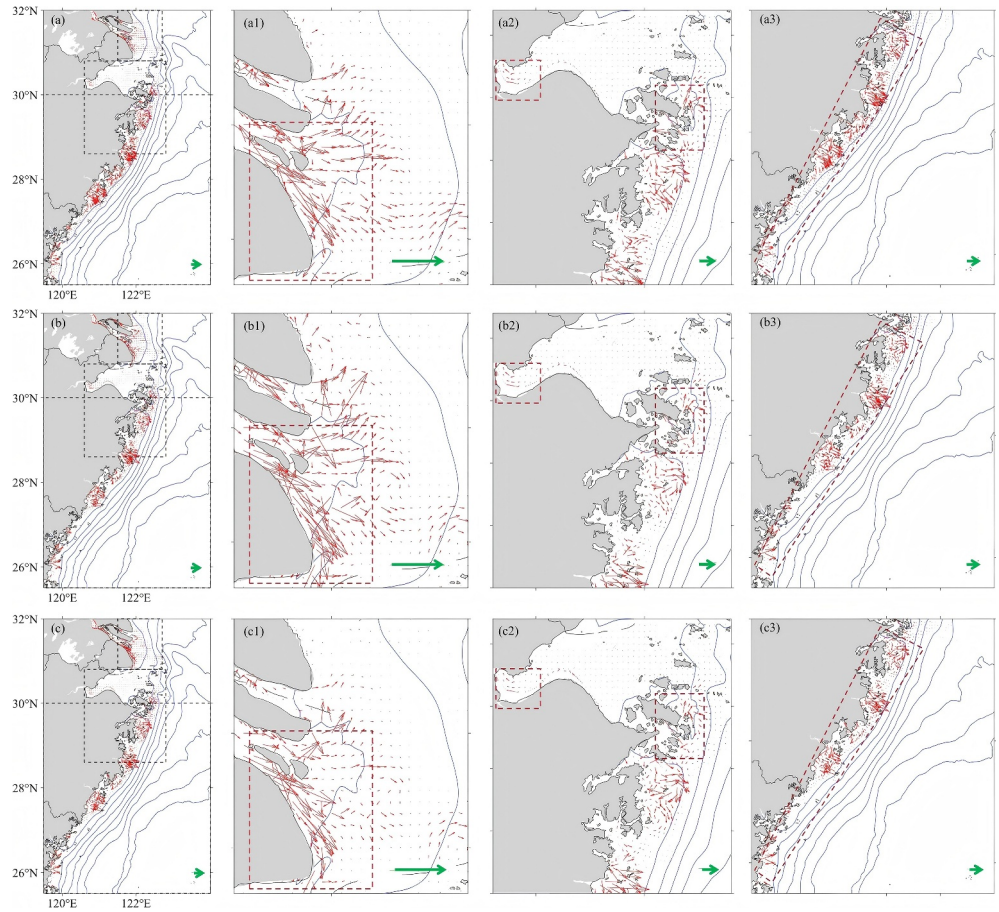

Figure 8. Sediment transport patterns under different typical TC tracks during 1949–1967. (a–c) Are types I, II, and III TCs, respectively. The black dashed area is enlarged to 1, 2, and 3 on the right. Brown dashed areas are sensitive areas, 1 is the southern branch of the Yangtze River Estuary; 2 is the head of Hangzhou Bay (left) and Zhoushan Island (right); and 3 is the Ningbo-Taizhou-Wenzhou line (from north to south) along the coast of Zhejiang and Fujian. The green arrow line represents 0.02 kg m^{-1} s^{-1} of net sediment transport flux.

Taizhou-Wenzhou line along the coast of Zhejiang and Fujian, where depth is shallower than 30 m, sediment transport is also active.

TCs from the third and second historical periods cause stronger net sediment transport than those from the first period due to poleward and shoreward shifts (Xu et al., 2024). The net sediment transport flux is highest along Track II, primarily due to its spatial characteristics. The typical position of Track II is closer to the ECCO than Track I (Figure 5). Meanwhile, the strongest portion of Track II is located further north, while Track I extends further southwest. This spatial difference results in stronger sediment transport intensity induced by Track II during the second and third historical periods in the ECCO region compared to that caused by Track I. In contrast, Track III demonstrates weaker net sediment transport as it is situated farther from the study area, over deeper waters. These spatial relationships suggest that Track II has a greater potential to cause sediment resuspension in the study region. The net sediment transport direction is mainly consistent with the wind direction during the TC. Among the nine scenarios simulating TC conditions, the ECCO area predominantly lies west of the TC center during peak intensity. Under these conditions, the prevailing TC winds originate primarily from the northwesterly and northerly directions. This consistent wind pattern results in minimal variations in sediment transport direction across different scenarios. Consequently, the net sediment transport direction in the four sensitive regions is primarily seaward and southward. By analyzing the historical net sediment transport patterns, the areas sensitive to TCs are identified. This provides a reference for the quantitative analysis of sediment transport during TCs.

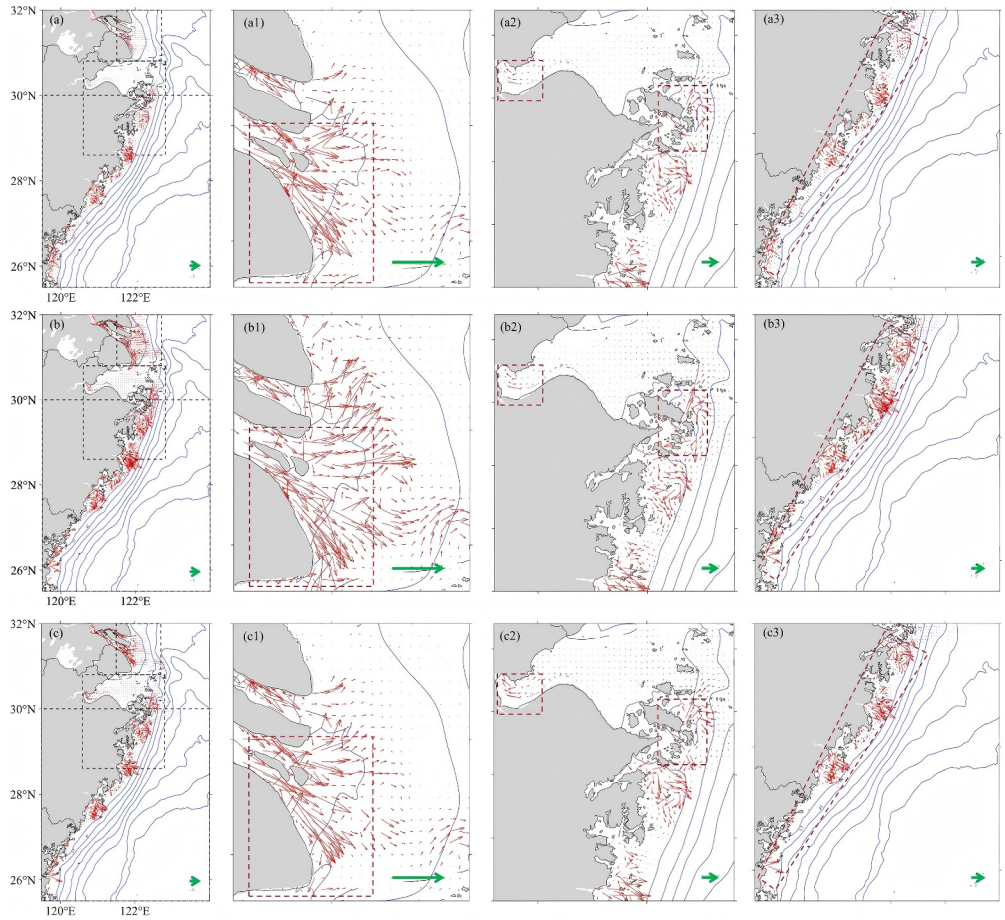

Figure 9. Sediment transport patterns under different typical TC tracks during 1968–1993. (a–c) Are type I, II, and III TCs, respectively. Brown dashed areas are sensitive areas. The black dashed area is enlarged to 1, 2, and 3 on the right. Brown dashed areas are sensitive areas; 1 is the southern branch of the Yangtze River estuary; 2 is the head of Hangzhou Bay (left) and Zhoushan Island (right); and 3 is the Ningbo-Taizhou-Wenzhou line (from north to south) along the coast of Zhejiang and Fujian. The green arrow line represents 0.02 kg m^{-1} s^{-1} of net sediment transport flux.

3.2. Erosion Distribution Under Latitudinal and Longitudinal Variation of Typhoon Tracks

3.2.1. Normal Conditions

In this section, the distribution of sediment at the peak TC intensity, which is defined as the moment of highest SSC during each TC, is considered according to the specific changes in latitude and longitude. The state of the seabed at this time is generally eroded (Figure 11). There is some deposition within the mouth of the Yangtze River, Zhoushan Islands, and along the coast of Zhejiang and Fujian. The erosional area extends from the TC eye to the surrounding area, and the magnitude of erosion gradually decreases away from the TC eye. The sediments along the coast of Zhejiang are fine-grained, with a small critical shear stress. When the TC eye gradually approaches this region, the change of erosion-deposition in this region is the strongest. As the TC track moves northward, the erosion in this region gradually decreases, and the erosion depth near Hangzhou Bay gradually increases. As the TC track moves further northward, erosion in the Yangtze River Estuary and its adjacent waters becomes stronger. The northward shift of the TC track leads to a gradual northward migration of the erosion area, with an increase in the erosion magnitude in the north and a decrease in the south part of the ECCO. The impact of TC landward shift is similar to that of poleward shift, in that TC-induced erosion deepens as the TC moves closer to the coast, with the mouth of the Yangtze River, Hangzhou Bay, and the coasts of Zhejiang and Fujian being the most significantly affected. The landward shift of TCs increases the risk of erosion in coastal areas.

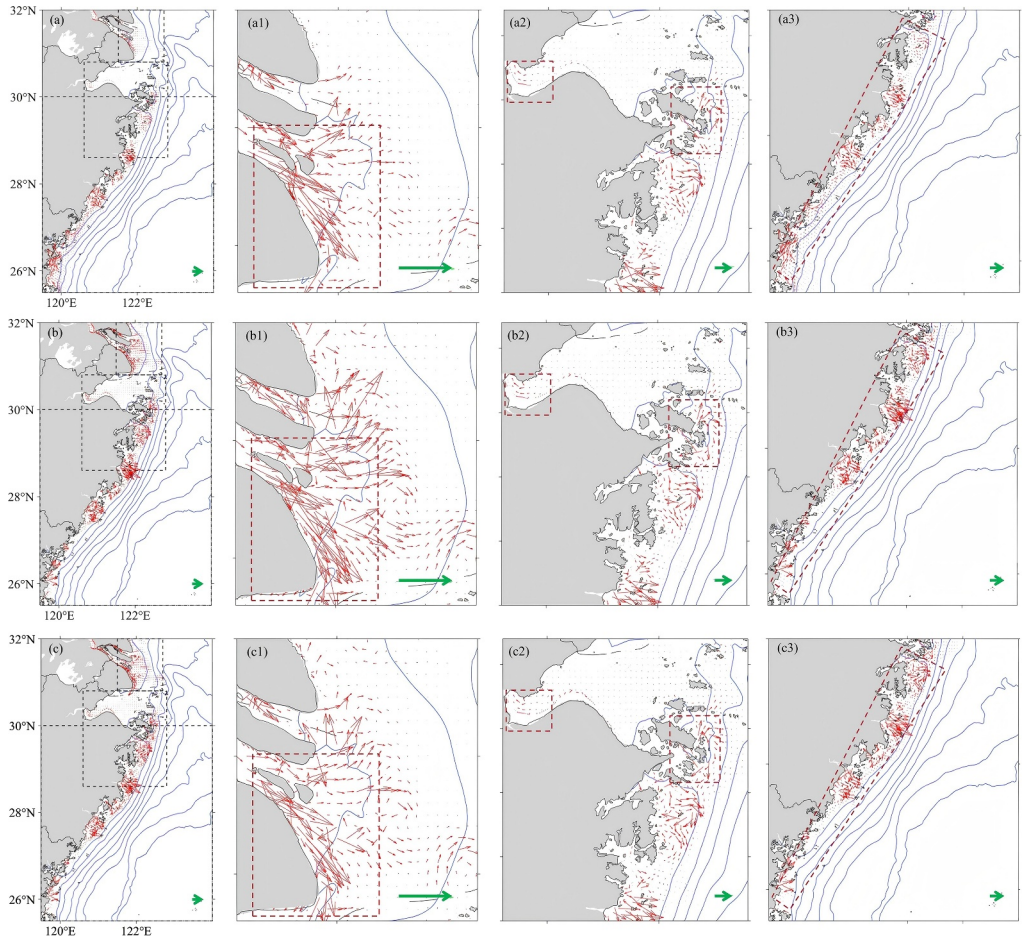

Figure 10. Sediment transport patterns under different typical TC tracks during 1994–2022. (a–c) Are type I, II, and III TCs, respectively. Brown dashed areas are sensitive areas. The black dashed area is enlarged to 1, 2, and 3 on the right. Brown dashed areas are sensitive areas; 1 is the southern branch of the Yangtze River Estuary; 2 is the head of Hangzhou Bay (left) and Zhoushan Island (right); and 3 is the Ningbo-Taizhou-Wenzhou line (from north to south) along the coast of Zhejiang and Fujian. The green arrow line represents 0.02 kg m^{-1} s^{-1} of net sediment transport flux.

3.2.2. Global Warming

At the peak intensity of TCs, the nearshore waters are predominantly characterized by erosion, which is further intensified under the influence of global warming (Figure 12). Figure 9 a1–e1 shows the difference in bed elevation between poleward-shifted TC tracks under global warming versus TC tracks under the present climate. Global warming leads to an increase in the intensity of TCs, and therefore, the erosion depth in the TC affected area is also significantly larger. The severely eroded area also shows the same pattern, in which the magnitude of erosion gradually decreases away from the TC center. As the TC track shifts poleward, the erosive area also shifts poleward; the erosion magnitude increased in the north, while in the south, the erosion magnitude changed less because it was generally further away from the TC.

Figure 12 a2–e2 shows the difference between the bed elevation changes of landward-shifted TC tracks under global warming versus under the present climate. Scenarios B2, B3, and B4 show severe erosion to the west of the TC. Scenario B5 shows a trend of decreasing erosion depth, but the magnitude of the change is small. Because the TC track in this scenario is farther away, the response to changes in the intensity of the TC is small. In this study, a slight trend of decreasing erosion depth is observed in scenario B5 due to the increased water depth that represents sea level rise, which leads to the weakening of bed shear stress. In scenario B1, the erosion depth on the right side of the tropical cyclone decreases, but the magnitude of the change is small. This is due to the weakening of the TC center in the north, as well as the fact that the area to the right of the track is mainly sand, for which the critical

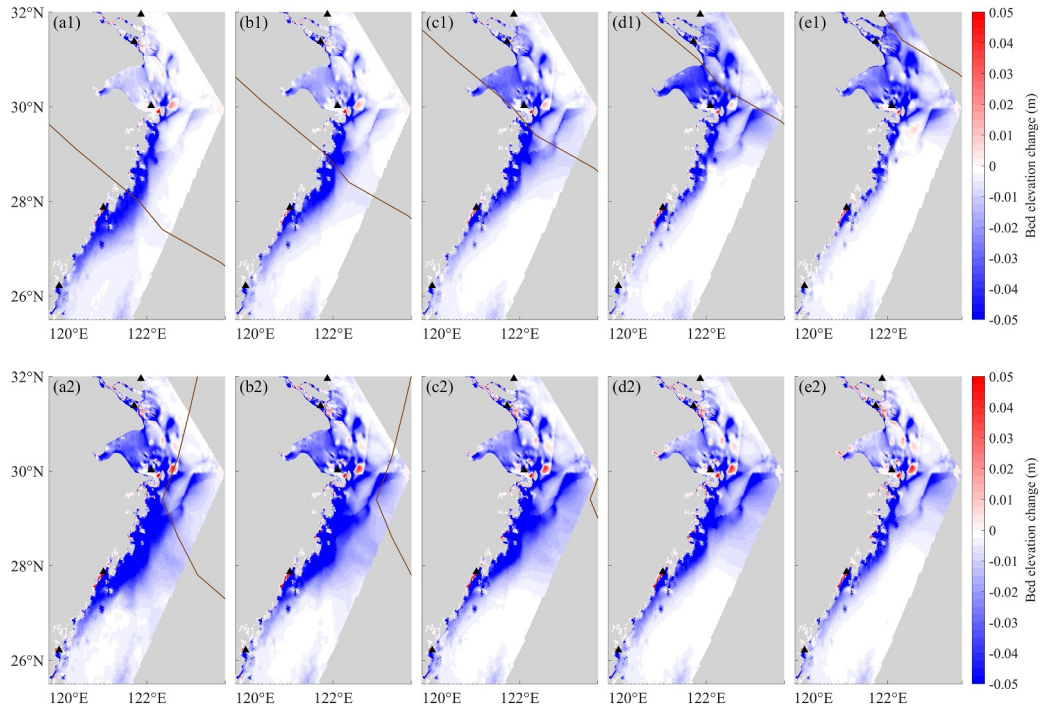

Figure 11. Bed elevation change during Typhoons 9711 and 1509 under latitudinal and longitudinal variation. a1–e1 show A1, A2, A3, A4, and A5, respectively, and a2–e3 show B1, B2, B3, B4, and B5, respectively.

shear stress of the sediment is set higher in the model (Figure 3), and the water depth is deeper. Combing these three factors makes the TC impact on this area weaker, with weak variability. Severe erosion is observed in the nearshore region, with more pronounced erosion depths on the left side of the TC track. It is concluded that global warming will still lead to strong erosion of nearshore waters.

4. Discussion

4.1. An Intuitive Perspective for the Analysis of TCs Change Impact

4.1.1. Effects of Latitudinal and Longitudinal Variation Based on Typical TC Tracks

TCs are extreme events with important impacts on the sedimentary environment of shallow shelves and nearshore waters (Zhu et al., 2020). The strong hydrodynamics caused by TCs can lead to strong sediment transport and large-scale erosion of the seabed. The sediments in the subaqueous delta of the Yangtze River have fine grain sizes and are easily resuspended under strong tidal currents. Especially under the influence of storm surges, hydrodynamic forces can affect areas as deep as 40 m, causing serious erosion or siltation changes in the underwater delta over a short time period (Dai, Liu, Wei, & Chen, 2014; Du et al., 2019). Section 3.1 identified four TC-sensitive sediment transport areas in the ECCO. Combining these with peak TC erosion patterns (Section 3.2), we selected 5 representative coastal sites (Qidong, Hengsha, Zhoushan, Wenzhou, and Fuzhou; Figure 6) for maximum erosion depth analysis. Using linear fitting (Fisher, 1925), we quantified erosion intensity relative to TC track position. This analysis provides an intuitive perspective into seabed erosion extent under future TC impacts. From Figure 13 a1–e1 and Table 2, the maximum erosion depths change by 0.25, 0.39, 1.63, 0.48, and 0.24 cm, respectively, when the TC track moves by 1° in latitude. Qidong is on the north side of the TC in the five scenarios, and Hengsha and Zhoushan are on the north side of the TC in the first four scenarios. The northward shift of the TC tracks makes these three stations closer to the TC, and thus, the erosion depth gradually deepens here. Wenzhou and Fuzhou, on the other hand, are on the south side of the TC tracks, so when the TC moves northward, the TC gradually moves away from these two stations, and thus the erosion depth decreases.

From Figure 13 a2–e2 and Table 3, when the TC moves 1° in longitude, the maximum erosion depths change by 0.05, 0.90, 1.06, and 0.08 cm, respectively. Since these five stations are located on the west side of the TC, the

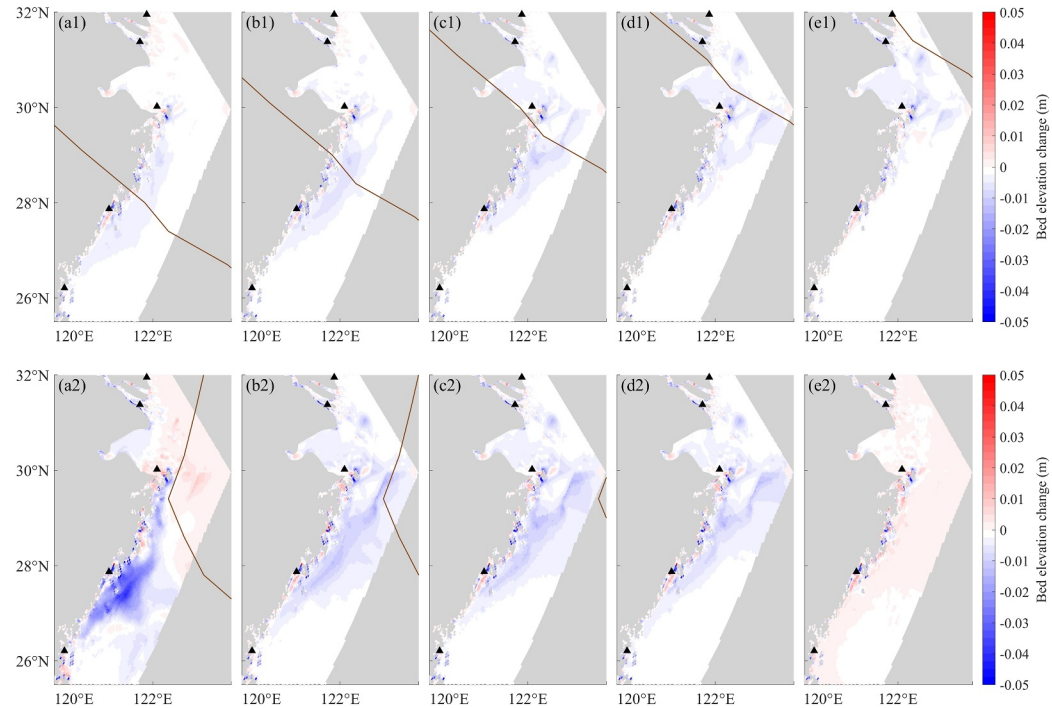

Figure 12. The difference in bed elevation change due to high suspended sediment concentration during Typhoons 9711 and 1509 from latitudinal and longitudinal variation under global warming. a1–e1 are A1, A2, A3, A4, and A5 under global warming, respectively; a2–e3 are B1, B2, B3, B4, and B5 under global warming, respectively.

westward shift of the TC track will bring these five stations closer to the TC, so the erosion depths are deepened except for Wenzhou. The Qidong and Fuzhou stations are farther away from the TC, so the changes in these two stations are smaller. The fluctuation of the erosion change at the Wenzhou station is larger because this station is farther away from the TC, and there are more islands around, so the response to the TC change is weaker and the trend of the erosion change is not obvious.

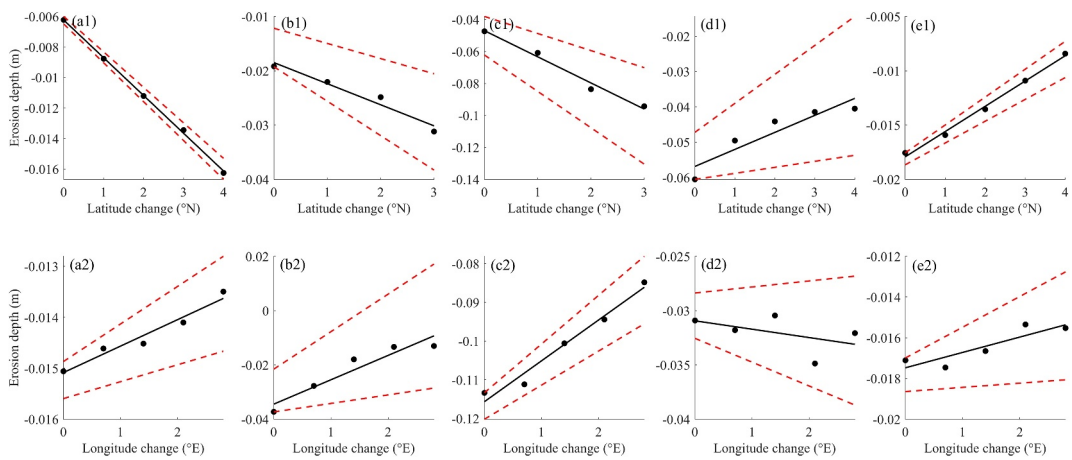

Figure 13. Maximum erosion depth at each station due to latitudinal and longitudinal variations of Typhoon 9711 and Typhoon 1509.

Table 2
Sensitivity of Maximum Erosion Depth to Latitudinal Variation

Station	Sensitive level	R	P
Qidong	-0.25 cm°N^{-1}	1.00	1.4×10^{-5}
Hengsha	-0.39 cm°N^{-1}	0.94	2.3×10^{-5}
Zhoushan	-1.63 cm°N^{-1}	0.98	0.9×10^{-5}
Wenzhou	$+0.48$ cm°N^{-1}	0.86	2.4×10^{-5}
Fouzhou	$+0.24$ cm°N^{-1}	0.99	2.2×10^{-5}

Note. Sensitivity level is the slope of the linear fit. (*p*-values indicating significance).

4.1.2. Effects of Global Warming Based on Typical TC

Global warming leads to an increase in the intensity of TCs as well as a rise in mean sea level (Section 3.2.2). Because many factors affect TC intensity, this study focuses on sedimentation changes due to TC intensity and track changes. We use the previously studied relationship between TC wind speed and temperature under average conditions, simplify TC changes under global warming, uniformly alter TCs with the formula above, and then intuitively analyze the impacts on sedimentation trends. The quantitative change in erosion due to this effect was further analyzed using the same method as in Section 4.1.1: The maximum erosion depths at these five stations during the time of strongest TC intensity were extracted and fitted to changes in latitude and longitude, thus deriving a quantitative relationship between changes in erosion depth due to changes in storm intensity as well as track latitude and longitude.

From Figure 14 a1-e1 and Table 4, it can be seen that a 1° shift in the latitude of the TC changes the maximum erosion depth by 0.27, 0.40, 1.67, 0.51, and 0.25 cm, respectively. Erosion depth increases compared to the present climate. Qidong, Hengsha, and Zhoushan are on the north side of the TC, so the poleward shift of the TC brings three stations closer to the TC. Sediment resuspension during the TC is enhanced, and the erosion depth increases with the poleward shift. Wenzhou and Fuzhou are located to the south of the TC, and their erosion depth gradually decreases with the poleward shift. Therefore, the poleward shift of TCs increases the probability of the northern coastal areas being exposed to the risk of TCs.

From Figure 14 a2-e2 and Table 5, the erosion depth on the western side of the TC deepens in scenarios B2, B3, and B4. Scenario B5 shows a trend of decreasing erosion depth, but the magnitude of this change is small. Because the TC is relatively far away in this scenario, the response to the change in TC intensity is small. In this study, slightly decreasing erosion depths occur due to increasing the water depth in the model to represent sea level rise, which leads to the weakening of bottom shear stresses (Xu, Wei, et al., 2022) in some scenarios. In scenario B1, the erosion depth on the right side of the TC decreases slightly. The nearshore of the ECCO (left of the TC) shows a deepening of erosion. It is concluded that global warming will still lead to stronger overall erosion caused by the westward shift of TC tracks. The maximum erosion depths change by 0.07, 1.02, 1.11, and 0.16 cm for a 1° shift in longitude of the TC. Qidong and Fuzhou, due to their small values of maximum erosion depth change, and experience a larger relative change than the present climate, with increases of 40% and 50%, respectively. The sensitivities of Hengsha and Zhoushan increased by 13.33% and 4.71%, respectively, compared with the present climate. The change in scour at the Wenzhou station is similar to that in Section 4.1.1 and still fluctuates considerably, while the trend of change in erosion is not obvious.

4.2. Future Impact of TC-Induced Erosion in the ECCO

Over the past half century, more than 50,000 dams have been built in the Yangtze River Basin, and sediment load has been reduced by 80%, resulting in a transition from deposition to erosion in the subaqueous delta of the Yangtze River at depths of less than 10 m (Li et al., 2015; Luan et al., 2017; Yang et al., 2011). The areas of ECCO deeper than 20 m water depth are less eroded under normal weather conditions (Xu, Wei, et al., 2022). From the historical sediment transport patterns in Section 3.1, it is clear that TCs can cause active sediment transport at water depths of around 30 m, with short-term strong erosion of the seabed occurring during the TC. Meanwhile, anthropogenic global warming can increase the sea surface temperature (SST) at low latitudes in the northwestern Pacific, leading to an increase in the energy available for TC generation (Mei et al., 2015; Mei & Xie, 2016). Higher SST can also lead to meridional expansion in the tropics (Sharmila & Walsh, 2018) to provide more theoretical energy for a poleward shift, which can further enhance the development of TCs. Changes in the steering airflow and vertical wind shear (VWS) also have an important impact on the movement and development of TCs. The steering flow can guide the direction of TC movement, and stronger VWS will lead to the restriction of TC development and its weakening of TC intensity (Camargo & Wing, 2021; Gray, 1968; Wang & Toumi, 2021).

Table 3
Sensitivity of Maximum Erosion Depth to Longitudinal Variation

Station	Sensitive level	R	P
Qidong	$+0.05$ cm°E^{-1}	0.95	1.7×10^{-5}
Hengsha	$+0.90$ cm°E^{-1}	0.90	1.5×10^{-2}
Zhoushan	$+1.06$ cm°E^{-1}	0.97	0.9×10^{-2}
Wenzhou	-0.08 cm°E^{-1}	0.25	9.3×10^{-5}
Fouzhou	$+0.08$ cm°E^{-1}	0.78	9.3×10^{-5}

Note. Sensitivity level is the slope of the linear fit.

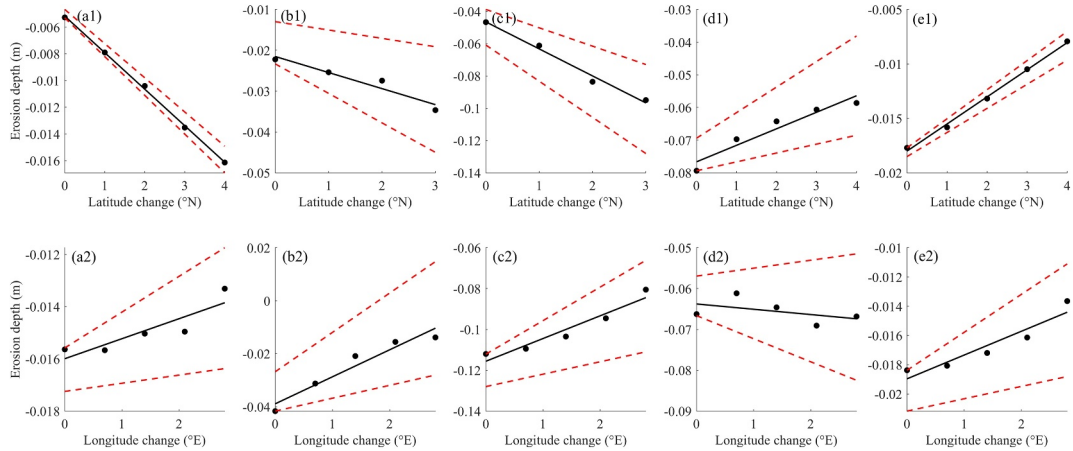

Figure 14. Maximum of erosion depth at each station about the latitudinal and longitudinal variation of Typhoon 9711 and Typhoon 1509 under global warming.

The westerly steering flow and VWS near ECCO are weakening, and the poleward and landward shift of TCs in this region will gradually increase as a result (Xu et al., 2024). Increased TC intensity and poleward and landward track shifts will further enhance resuspension of seabed sediment in the study area during TCs. Sediment transport in areas of ECCO shallower than 30 m may become more active in the future, with further enhancement of strong erosion during TCs. The deepening of erosion is more obvious in the near shore due to the shallower water depth. In deeper waters to the east of the TC tracks, erosion weakens due to increased water depth, but overall erosion in ECCO is still enhanced. To summarize, under the present climate, areas shallower than 10 m have a higher risk of erosion due to the influence of reduced sediment load, while areas shallower than 30 m have a higher risk of disturbance due to the impact of TCs. Areas at risk may include those deeper than 30 m in the future as a result of changes in TC intensity and track. The poleward and landward migration of TCs is an ongoing global phenomenon. Given the enormous destructive power of TCs, combining the analysis of regional TC track shift proposed in this study to understand the quantitative impacts and scope of TCs in local regions, and to carry out disaster prevention and mitigation planning for areas severely affected by TCs, and provides clues for the adjustment of planning for disaster prevention in the coastal zone.

4.3. Advantages and Improvements of the Coupled Delft3D-FM Model

Simulation of sediment transport processes is more challenging than hydrodynamic processes, and accurate representation of sediment properties in the model is important (Tang et al., 2023). Because this study focuses more on the sediment transport response on a larger scale, only one layer of the cohesive sediment fraction is set up in this model. To ensure the correct setting of the sediment parameters, the model in this study was calibrated using measured sediment data, including sediment dry bed density measured from the study area (Xue et al., 2020), cohesive sediment critical shear stress and erosivity from measured data (Xu, Wei, et al., 2022), and empirically determined critical shear stress and erosivity of sand (Chen et al., 2021), to construct the spatial distribution of the sediment properties in the Yangtze River Estuary, Hangzhou Bay, and Zhejiang and Fujian coasts. This ensures the reliability of the model simulation. Follow-up studies should simulate geomorphic evolution and stratigraphic sequences in response to multiple sediment types and multiple layers of sediments for horizontal spatial variability and vertical grain-size stratification (Xing et al., 2024). This would help us understand land-sea interactions in critical zones and have important implications for the regional environment and sustainable development.

This study used a two-dimensional depth-averaged model (Liu et al., 2023; Luan et al., 2017; Xing et al., 2024) and did not consider three-dimensional

Table 4
Sensitivity of Maximum Erosion Depth to Latitudinal Variation Under Global Warming

Station	Sensitivity level	Range	R	P
Qidong	-0.27 cm°N^{-1}	+8.00%	1.00	1.7×10^{-5}
Hengsha	-0.40 cm°N^{-1}	+2.56%	0.93	3.7×10^{-2}
Zhoushan	-1.67 cm°N^{-1}	+2.45%	0.99	7.0×10^{-3}
Wenzhou	+0.51 cm°N^{-1}	+6.25%	0.92	9.0×10^{-3}
Fouzhou	+0.25 cm°N^{-1}	+4.17%	0.99	9.2×10^{-4}

Note. Sensitivity level is the slope of the linear fit.

Table 5
Sensitivity of Maximum Erosion Depth to Longitudinal Variation Under Global Warming

Station	Sensitivity level	Range	R	P
Qidong	+0.07 cm°E^{-1}	+40.00%	0.78	4.6×10^{-5}
Hengsha	+1.02 cm°E^{-1}	+13.33%	0.93	8.0×10^{-3}
Zhoushan	+1.11 cm°E^{-1}	+4.71%	0.91	9.0×10^{-3}
Wenzhou	−0.13 cm°E^{-1}	+6.25%	0.92	9.0×10^{-3}
Fouzhou	+0.16 cm°E^{-1}	+50.00%	0.89	1.6×10^{-2}

Note. Sensitivity level is the slope of the linear fit.

processes in the estuary, such as gravitational circulation or density stratification, as these processes require a three-dimensional model to simulate vertical changes (Wu et al., 2012). In addition, vertical stratification due to salinity, temperature, and suspended sediments in estuarine waters (Simpson et al., 1990) as well as global warming-induced stratification of seawater can affect turbulent mixing and consequently affect sediment transport (Tan et al., 2022; Tian et al., 2023). However, the three-dimensional model, although more accurate, is substantially less computationally efficient and its enhancement is inconclusive (Luan et al., 2017). As model complexity increases, accuracy may decrease and interpretation of model results becomes more difficult (Van, 2011). The coupled model in this study has been able to reproduce the vertically averaged flow field with high reliability while saving computational time. Seasonal variations in Yangtze River runoff also play a role in the geomorphologic evolution of the Yangtze River Estuary and its adjacent seas (Luan et al., 2017; Zhu et al., 2020); the present study used the multiyear average runoff and SSC at the Datong station, which is lower than the peak flood runoff and smooths out the peak value. When conducting region-specific simulation studies, it is necessary to carry out further three-dimensional simulation studies based on the current coupled model and discuss the accuracy of the complex model by considering different flow and sediment loads in comparison with the two-dimensional model results.

5. Conclusion

Focused on the ECCO, a region severely affected by TCs, this study utilizes the Delft3D-FM numerical model integrated with TC best track data and field measurements to investigate sediment transport patterns under historical TC tracks and to quantify erosion responses to poleward and landward track shifts. The main conclusions of the study are summarized below:

There are four distinct zones in the ECCO exhibiting the most active net sediment transport under typical historical TC tracks: The area of the Yangtze River Delta with a water depth of 20 m or less, especially shallower than 10 m in the southern branch of the Yangtze River Estuary, is heavily affected. The net sediment transport in Hangzhou Bay is weaker, with the sediment activity in the area with a water depth of 10 m or less at the top of the bay being the most active area in Hangzhou Bay. Sediment transport is more active in the area with a water depth of 20–30 m on the east side of the Zhoushan Islands. Along the coast of Zhejiang and Fujian, sediment transport is active in areas with water depths as deep as 30 m. In short, from the historical sediment transport pattern derived from the typical historical TC track, results reveal that sediment in waters shallower than 30 m is highly sensitive to TC activity.

The latitudinal and longitudinal impacts on the poleward and landward migration of typical TC tracks I and II, respectively, will lead to northward and westward shifts of the erosion centers of TCs. This will increase the risk of TC hazards for northern coastal areas, and global warming will cause the northern coastal areas to face a further increase in the risk of TC hazards in the future. Coastal erosion depth changes due to poleward and landward shifts based on typical TC tracks I and II during the peak TC intensity period are quantified as 0.24–1.63 cm°N^{-1} and 0.05–1.06 cm°E^{-1}, respectively. Under the future global warming condition (4°C temperature increase and 1.1-m sea level rise set in this study), these values along the ECCO are projected to be 0.27–1.67 cm°N^{-1} and 0.07–1.11 cm°E^{-1}, increases of 2.45%–8.00% and 4.71%–13.33%, respectively.

Conflict of Interest

The authors declare no conflicts of interest relevant to this study.

Data Availability Statement

The model input files and validation data are available at https://zenodo.org/records/15073829.

Acknowledgments
The works presented in this paper is financially sponsored by the National Natural Science Foundation of China (52171260), National Key R&D Program of China (2024YFB2605900), National Natural Science Foundation of China (42276050, U2240220, and 41876092); the US National Science Foundation (Grant 2228486 and 2228485).

References

Al-Attabi, Z., Xu, Y., Tso, G., & Narayan, S. (2023). The impacts of tidal wetland loss and coastal development on storm surge damages to people and property: A Hurricane Ike case-study. *Scientific Reports*, *13*(1), 4620. https://doi.org/10.1038/s41598-023-31409-x

Atkinson, G. D., & Holliday, C. R. (1977). Tropical cyclone minimum sea level pressure/maximum sustained wind relationship for the Western North Pacific. *Monthly Weather Review*, *105*(4), 421–427. https://doi.org/10.1175/1520-0493(1977)105<0421:tcmslp>2.0.co;2

Calvin, K., Dasgupta, D., Krinner, G., et al. (2023). Sections. In *Climate change 2023: Synthesis report. Contribution of working groups I, II and III to the sixth assessment report of the intergovernmental Panel on climate change* (1st ed.). Intergovernmental Panel on Climate Change (IPCC).

Camargo, S. J., & Wing, A. A. (2021). Increased tropical cyclone risk to coasts. *Science*, *371*(6528), 458–459. https://doi.org/10.1126/science.abg3651

Chen, Y. W., Sheng, H., Xu, H. Q., et al. (2021). Analysis of sediment grain size change and its response to erosion and deposition pattern within the Yangtze River Estuary for the past 40 years. *Hydro-Science and Engineering*, *5*, 8–18.

Dai, Z., Liu, J. T., Wei, W., & Chen, J. (2014). Detection of the three gorges dam influence on the changjiang (Yangtze River) submerged delta. *Scientific Reports*, *4*(1), 6600. https://doi.org/10.1038/srep06600

Dai, Z.-J., Liu, J. T., Xie, H., & Shi, W. y. (2014). Sedimentation in the outer Hangzhou bay, China: The influence of Changjiang sediment load. *Journal of Coastal Research*, *298*, 1218–1225. https://doi.org/10.2112/jcoastres-d-12-00164.1

Deltares. (2022a). *D-flow flexible mesh user manual*. Deltares.

Deltares, D. (2022b). *Waves user manual*. Deltares.

Diaz Loaiza, M. A., Bricker, J. D., Meynadier, R., Duong, T. M., Ranasinghe, R., & Jonkman, S. N. (2022). Development of damage curves for buildings near La Rochelle during storm Xynthia based on insurance claims and hydrodynamic simulations. *Natural Hazards and Earth System Sciences*, *22*(2), 345–360. https://doi.org/10.5194/nhess-22-345-2022

Du, J., Park, K., Dellapenna, T. M., & Clay, J. M. (2019). Dramatic hydrodynamic and sedimentary responses in Galveston Bay and adjacent inner shelf to Hurricane Harvey. *Science of The Total Environment*, *653*, 554–564. https://doi.org/10.1016/j.scitotenv.2018.10.403

Dyer, K. R. (1997). *Estuaries-a physical introduction* (second ed edition). Wiley.

Egbert, G. D., & Erofeeva, S. Y. (2002). Efficient inverse modeling of Barotropic Ocean tides. *Journal of Atmospheric and Oceanic Technology*, *19*(2), 183–204. https://doi.org/10.1175/1520-0426(2002)019<0183:eimobo>2.0.co;2

Emanuel, K. (1986). An air-sea interaction theory for tropical cyclones. Part I: Steady-state maintenance. *Journal of the Atmospheric Sciences*, *43*(6), 585–605. https://doi.org/10.1175/1520-0469(1986)043<0585:aasitf>2.0.co;2

Emanuel, K. (2003). Tropical cyclones. *Annual Review of Earth and Planetary Sciences*, *31*(1), 75–104. https://doi.org/10.1146/annurev.earth.31.100901.141259

Fisher, R. A. (1925). *Statistical methods for research workers*. Oliver & Boyd.

Gao, S., & Collins, M. B. (2014). Holocene sedimentary systems on continental shelves. *Marine Geology*, *352*, 268–294. https://doi.org/10.1016/j.margeo.2014.03.021

Gao, S., Jia, J. J., Yang, Y., et al. (2019). Obtaining typhoon information from sedimentary records in coastal-shelf waters. *Hai Yang Xue Bao*, *41*(10), 141–160.

Gray, W. M. (1968). Global view of the origin of tropical disturbances and storms. *Monthly Weather Review*, *96*(10), 669–700. https://doi.org/10.1175/1520-0493(1968)096<0669:gvotoo>2.0.co;2

Guo, J. (2020). Empirical model for shields diagram and its applications. *Journal of Hydraulic Engineering*, *146*(6), 04020038. https://doi.org/10.1061/(asce)hy.1943-7900.0001739

Guo, W., Yao, D., Chen, Z., Ding, P., & Ge, J. (2023). Assessment of future flood risk induced by sea level rise and tropical cyclones under global warming in the Xiamen Bay, Fujian, China. *Frontiers in Marine Science*, *10*, 1103279. https://doi.org/10.3389/fmars.2023.1103279

Hawkes, A. D., & Horton, B. P. (2012). Sedimentary record of storm deposits from hurricane Ike, Galveston and san Luis Islands, Texas. *Geomorphology*, *171*, 180–189. https://doi.org/10.1016/j.geomorph.2012.05.017

Helderop, E., & Grubesic, T. H. (2019). Social, geomorphic, and climatic factors driving U.S. coastal city vulnerability to storm surge flooding. *Ocean and Coastal Management*, *181*, 104902. https://doi.org/10.1016/j.ocecoaman.2019.104902

Holland, G. (2008). A revised hurricane pressure–wind model. *Monthly Weather Review*, *136*(9), 3432–3445. https://doi.org/10.1175/2008mwr2395.1

Holland, G. J. (1980). An analytic model of the wind and pressure profiles in hurricanes. *Monthly Weather Review*, *108*(8), 1212–1218. https://doi.org/10.1175/1520-0493(1980)108<1212:aamotw>2.0.co;2

Hu, K., Ding, P., Wang, Z., & Yang, S. (2009). A 2D/3D hydrodynamic and sediment transport model for the Yangtze Estuary, China. *Journal of Marine Systems*, *77*(1–2), 114–136. https://doi.org/10.1016/j.jmarsys.2008.11.014

IPCC. (2022). *The Ocean and cryosphere in a changing climate: Special report of the intergovernmental Panel on climate change* (1 edition). Cambridge University Press.

Jia, X., Lu, C. T., & Huang, H. C. (2017). The extraordinary weather process inducing sudden siltation in deepwater navigation channel of Yangtze Estuary II: Sensitivity analysis of typhoon parameters and its typical tracks. *Journal of Hohai University(Natural Sciences)*, *45*(5), 439–444.

Ke, Q., Yin, J., Bricker, J. D., Savage, N., Buonomo, E., Ye, Q., et al. (2021). An integrated framework of coastal flood modelling under the failures of sea dikes: A case study in Shanghai. *Natural Hazards*, *109*(1), 671–703. https://doi.org/10.1007/s11069-021-04853-z

Knutson, T., Camargo, S. J., Chan, J. C. L., Emanuel, K., Ho, C. H., Kossin, J., et al. (2019). Tropical cyclones and climate change assessment: Part I: Detection and attribution. *Bulletin of the American Meteorological Society*, *100*(10), 1987–2007. https://doi.org/10.1175/bams-d-18-0189.1

Knutson, T., Camargo, S. J., Chan, J. C. L., Emanuel, K., Ho, C. H., Kossin, J., et al. (2020). Tropical cyclones and climate change assessment: Part II: Projected response to anthropogenic warming. *Bulletin of the American Meteorological Society*, *101*(3), E303–E322. https://doi.org/10.1175/bams-d-18-0194.1

Kossin, J. P., Emanuel, K. A., & Camargo, S. J. (2016). Past and projected changes in western North pacific tropical cyclone exposure. *Journal of Climate*, *29*(16), 5725–5739. https://doi.org/10.1175/jcli-d-16-0076.1

Kossin, J. P., Emanuel, K. A., & Vecchi, G. A. (2014). The poleward migration of the location of tropical cyclone maximum intensity. *Nature*, *509*(7500), 349–352. https://doi.org/10.1038/nature13278

Li, B., Yan, X. X., He, Z. F., Zhang, J., & Chen, Y. (2015). Impacts of the three gorges dam on the bathymetric evolution of the Yangtze River Estuary. *China Science Bulletin (in Chinese)*, *60*(18), 1736–1745. https://doi.org/10.1360/n972014-01074

Li, L., & Chakraborty, P. (2020). Slower decay of landfalling hurricanes in a warming world. *Nature*, *587*(7833), 230–234. https://doi.org/10.1038/s41586-020-2867-7

Liu, X., Xing, F., Shi, B., Wu, G., Ge, J., Peng, B., et al. (2023). Erosion and accretion patterns on intertidal mudflats of the Yangtze River Estuary in response to storm conditions. *Anthropocene Coasts*, *6*(1), 6. https://doi.org/10.1007/s44218-023-00020-y

Lu, J., Jiang, J., Li, A., & Ma, X. (2018). Impact of Typhoon Chan-hom on the marine environment and sediment dynamics on the inner shelf of the East China Sea: In situ seafloor observations. *Marine Geology*, *406*, 72–83. https://doi.org/10.1016/j.margeo.2018.09.009

Lu, X., Yu, H., Ying, M., Zhao, B., Zhang, S., Lin, L., et al. (2021). Western North Pacific tropical cyclone database created by the China meteorological administration. *Advances in Atmospheric Sciences*, *38*(4), 690–699. https://doi.org/10.1007/s00376-020-0211-7

Luan, H. L., Ding, P. X., Wang, Z. B., & Ge, J. Z. (2017). Process-based morphodynamic modeling of the Yangtze Estuary at a decadal timescale: Controls on estuarine evolution and future trends. *Geomorphology*, *290*, 347–364. https://doi.org/10.1016/j.geomorph.2017.04.016

Makin, V. K. (2005). A note on the drag of the sea surface at hurricane winds. *Boundary-Layer Meteorology*, *115*(1), 169–176. https://doi.org/10.1007/s10546-004-3647-x

Mei, W., & Xie, S.-P. (2016). Intensification of landfalling typhoons over the northwest Pacific since the late 1970s-supporting. *Nature Geoscience*, *9*(10), 753–757. https://doi.org/10.1038/ngeo2792

Mei, W., Xie, S.-P., Primeau, F., McWilliams, J. C., & Pasquero, C. (2015). Northwestern Pacific typhoon intensity controlled by changes in ocean temperatures. *Science Advances*, *1*(4), e1500014. https://doi.org/10.1126/sciadv.1500014

Mo, D., Wang, N., & Hu, P. (2024). Hazard assessment of dynamic marine processes during two extreme weather systems near the Shandong Peninsula. *Journal of Sea Research*, *201*, 102520. https://doi.org/10.1016/j.seares.2024.102520

Muis, S., Verlaan, M., Winsemius, H. C., Aerts, J. C. J. H., & Ward, P. J. (2016). A global reanalysis of storm surges and extreme sea levels. *Nature Communications*, *7*(1), 11969. https://doi.org/10.1038/ncomms11969

Ren, J., Xu, F., He, Q., Shen, J., Guo, L., Xie, W., & Zhu, L. (2021). The role of a remote tropical cyclone in sediment resuspension over the subaqueous delta front in the Changjiang Estuary, China. *Geomorphology*, *377*, 107564. https://doi.org/10.1016/j.geomorph.2020.107564

Schenkel, B. A., & Hart, R. E. (2012). An examination of tropical cyclone position, intensity, and intensity life cycle within atmospheric reanalysis datasets. *Journal of Climate*, *25*(10), 3453–3475. https://doi.org/10.1175/2011jcli4208.1

Schuerch, M., Dolch, T., Reise, K., & Vafeidis, A. T. (2014). Unravelling interactions between salt marsh evolution and sedimentary processes in the Wadden Sea (Southeastern North Sea). *Progress in Physical Geography: Earth and Environment*, *38*(6), 691–715. https://doi.org/10.1177/0309133314548746

Shan, K., Lin, Y., Chu, P.-S., Yu, X., & Song, F. (2023). Seasonal advance of intense tropical cyclones in a warming climate. *Nature*, *623*(7985), 83–89. https://doi.org/10.1038/s41586-023-06544-0

Sharmila, S., & Walsh, K. J. E. (2018). Recent poleward shift of tropical cyclone formation linked to Hadley cell expansion. *Nature Climate Change*, *8*(8), 730–736. https://doi.org/10.1038/s41558-018-0227-5

Shi, X. F. (2012). *Marine sedimentation of China marginal seas (in Chinese)*. Ocean press.

Simpson, J. H., Brown, J., Matthews, J., & Allen, G. (1990). Tidal straining, density currents, and stirring in the control of estuarine stratification. *Estuaries*, *13*(2), 125–132. https://doi.org/10.2307/1351581

SOA, (1997). *Chinese Marine Disaster Communique In 1997 (In Chinese)*.

Studholme, J., Fedorov, A. V., Gulev, S. K., Emanuel, K., & Hodges, K. (2022). Poleward expansion of tropical cyclone latitudes in warming climates. *Nature Geoscience*, *15*(1), 14–28. https://doi.org/10.1038/s41561-021-00859-1

Takagi, H., & Wu, W. (2016). Maximum wind radius estimated by the 50 kt radius: Improvement of storm surge forecasting over the Western North Pacific. *Natural Hazards and Earth System Sciences*, *16*(3), 705–717. https://doi.org/10.5194/nhess-16-705-2016

Tan, H. J., Cai, R. S., Du, J. G., et al. (2022). Climate change and marine ecosystem: Impacts, adaptation, and vulnerability. *Transactions of Atmospheric Sciences (in Chinese)*, *45*(4), 489–501.

Tang, B., Zhang, F., Jia, J., Feng, Z., Tang, J., Xing, F., & Wang, Y. P. (2023). The role of tropical cyclone on Changjiang River subaqueous delta geomorphology: A numerical investigation of tropical cyclone Danas (2019). *Journal of Geophysical Research: Oceans*, *128*(5), e2022JC019190. https://doi.org/10.1029/2022jc019190

Thompson, R. O. R. Y. (1983). Low-pass filters to suppress inertial and tidal frequencies. *Journal of Physical Oceanography*, *13*(6), 1077–1083. https://doi.org/10.1175/1520-0485(1983)013<1077:lpftsi>2.0.co;2

Tian, J., Zhang, F., Li, R. Z., et al. (2023). Observation and analysis of turbulence vertical profile in the Changjiang river estuary. *Ocaeanologia et Limnologia Sinica (in Chinese)*, *54*(5), 1295–1307.

Van, R. (2011). Coastal erosion and control. *Ocean and Coastal Management*, *54*(12), 867–887. https://doi.org/10.1016/j.ocecoaman.2011.05.004

Veeramony, J., Condon, A., & Van Ormondt, M. (2017). Forecasting storm surge and inundation: Model validation. *Weather and Forecasting*, *32*(6), 2045–2063. https://doi.org/10.1175/waf-d-17-0015.1

Walters, R. A., & Heston, C. (1982). Removing tidal-period variations from time-series data using low-pass digital filters. *Journal of Physical Oceanography*, *12*(1), 112–115. https://doi.org/10.1175/1520-0485(1982)012<0112:rtpvft>2.0.co;2

Wang, B., & Song, Y. (2011). Study on the difference of amorphous substances of coal ashes. *Advanced Materials Research*, *287*, 1189–1192. https://doi.org/10.4028/www.scientific.net/amr.287-290.1189

Wang, N., Hou, Y., Mo, D., & Li, J. (2021). Hazard assessment of storm surges and concomitant waves in Shandong Peninsula based on long-term numerical simulations. *Ocean and Coastal Management*, *213*, 105888. https://doi.org/10.1016/j.ocecoaman.2021.105888

Wang, S., & Toumi, R. (2021). Recent migration of tropical cyclones toward coasts. *Science*, *371*(6528), 514–517. https://doi.org/10.1126/science.abb9038

Willmott, C. J. (1981). On the validation of models. *Physical Geography*, *2*(2), 184–194. https://doi.org/10.1080/02723646.1981.10642213

Wu, J., Liu, J. T., & Wang, X. (2012). Sediment trapping of turbidity maxima in the Changjiang Estuary. *Marine Geology*, *303–306*, 14–25. https://doi.org/10.1016/j.margeo.2012.02.011

Xing, F., Wang, Y. P., Ni, W., Gao, S., Jia, J., & Gao, J. (2024). Modeling multi-decadal morphological evolution of the radial-shaped sand ridges in the Southern Yellow Sea, China. *CATENA*, *238*, 107884. https://doi.org/10.1016/j.catena.2024.107884

Xu, C., Nelson-Mercer, B., Bricker, J., Davlasheridze, M., Ross, A. D., & Jia, J. (2023). Damage curves derived from hurricane Ike in the west of Galveston bay based on insurance claims and hydrodynamic simulations. *International Journal of Disaster Risk Science*, *14*(6), 932–946. https://doi.org/10.1007/s13753-023-00524-8

Xu, C., Wei, D., Chen, Y., Yang, Y., Zhang, F., Wang, Y. P., & Jia, J. (2022). Sediment erodibility in the Changjiang (Yangtze) subaqueous delta: Spatial–temporal distribution and sedimentary significance. *Anthropocene Coasts*, *5*(1), 10. https://doi.org/10.1007/s44218-022-00011-5

Xu, C., Yang, Y., Jia, J., Bricker, J. D., & Wang, Y. P. (2024). A 70-year record reveals the poleward shift of tropical cyclone tracks in the east China coastal ocean is twice that of landward shift. *Global and Planetary Change*, *242*, 104566. https://doi.org/10.1016/j.gloplacha.2024.104566

Xu, C., Yang, Y., Zhang, F., Li, R., Li, Z., Wang, Y. P., & Jia, J. (2022). Spatial-temporal distribution of tropical cyclone activity on the eastern sea area of China since the late 1940s. *Estuarine, Coastal and Shelf Science*, *277*, 108067. https://doi.org/10.1016/j.ecss.2022.108067

Xu, H., Tian, Z., Sun, L., Ye, Q., Ragno, E., Bricker, J., et al. (2022). Compound flood impact of water level and rainfall during tropical cyclone periods in a coastal city: The case of Shanghai. *Natural Hazards and Earth System Sciences*, *22*(7), 2347–2358. https://doi.org/10.5194/nhess-22-2347-2022

Xu, S., & Huang, W. (2011). Estimating extreme water levels with long-term data by GEV distribution at Wusong station near Shanghai city in Yangtze Estuary. *Ocean Engineering*, *38*(2–3), 468–478. https://doi.org/10.1016/j.oceaneng.2010.11.022

Xu, Y., Xing, F., Cheng, J., Zhang, F., He, H., Zhang, J., et al. (2023). Sediment exchange between southern yellow sea and Yangtze river Estuary in response to storm events. *Estuarine, Coastal and Shelf Science*, *293*, 108508. https://doi.org/10.1016/j.ecss.2023.108508

Xue, C. F., Sheng, H., Wei, D. Y., et al. (2020). Dry bulk density analysis for inner shelf sediments of the East China sea and its sedimentary implications. *Ocaeanologia et Limnologia Sinica (in Chinese)*, *51*(5), 1093–1107.

Yang, S. L., Milliman, J. D., Li, P., & Xu, K. (2011). 50,000 dams later: Erosion of the Yangtze River and its delta. *Global and Planetary Change*, *75*(1–2), 14–20. https://doi.org/10.1016/j.gloplacha.2010.09.006

Yin, K., Li, R., Xu, S., et al. (2019). Influence of typhoon induced siltation on waterway transportation in navigation channel of guan River Estuary//CICTP 2019. *American Society of Civil Engineers*, 148–158.

Ying, M., Zhang, W., Yu, H., Lu, X., Feng, J., Fan, Y., et al. (2014). An overview of the China meteorological administration tropical cyclone database. *Journal of Atmospheric and Oceanic Technology*, *31*(2), 287–301. https://doi.org/10.1175/jtech-d-12-00119.1

Zhao, H., Wu, L., & Wang, R. (2014). Decadal variations of intense tropical cyclones over the western North Pacific during 1948–2010. *Advances in Atmospheric Sciences*, *31*(1), 57–65. https://doi.org/10.1007/s00376-013-3011-5

Zhao, H., Zhao, K., Klotzbach, P. J., Chand, S. S., Camargo, S. J., Cao, J., & Wu, L. (2024). Decreasing global tropical cyclone frequency in CMIP6 historical simulations. *Science Advances*, *10*(27), eadl2142. https://doi.org/10.1126/sciadv.adl2142

Zhu, B., Li, Y., Yue, Y., Yang, Y., Liang, E., Zhang, C., & Borthwick, A. G. L. (2020). Alternate erosion and deposition in the Yangtze Estuary and the future change. *Journal of Geographical Sciences*, *30*(1), 145–163. https://doi.org/10.1007/s11442-020-1720-0

Zou, P. X., Bricker, J. D., & Uijttewaal, W. S. J. (2020). Impacts of extreme events on hydrodynamic characteristics of a submerged floating tunnel. *Ocean Engineering*, *218*, 108221. https://doi.org/10.1016/j.oceaneng.2020.108221